Review

International Journal of Modern Physics D
Vol. 28, No. 1 (2019) 1930002 (21 pages)

DOI: 10.1142/S0218271819300027

World Scientific
www.worldscientific.com

Interpreting deviations between AR-VTG and GR

Roberto Dale

Departament d'Estadísica, Matemàtiques i Informàtica,
Universitat Miguel Hernández, Elx, E-03202 Alacant, Spain

Center of Operations Research (CIO),
University Miguel Hernandez of Elche (UMH),
Elx, E-03202 Alacant, Spain
rdale@umh.es

Diego Sáez

Departamento de Astronomía y Astrofísica,
Universidad de Valencia, Burjassot, E-46100 Valencia, Spain

Observatorio Astronómico, Universidad de Valencia,
Paterna, E-46980 Valencia, Spain
diego.saez@uv.es

Received 16 April 2018
Revised 19 July 2018
Accepted 27 August 2018
Published 18 September 2018

The cosmic microwave background (CMB) anisotropies predicted by two cosmological models are compared, one of them is the standard model of general relativity with cold dark matter and cosmological constant, whereas the second model is based on a consistent vector-tensor theory of gravitation explaining solar system and cosmological observations. It is proved that the resulting differences — between the anisotropies of both models — are due to the so-called late integrated Sachs–Wolfe effect and, consequently, cross-correlations between maps of CMB temperatures and tracers of the dark matter distribution could be used in future to select one of the above models. The role of reionization is analyzed in detail.

Keywords: Modified theories of gravity; cosmology: late integrated Sachs–Wolfe.

PACS Number(s): 04.50.Kd, 98.65.−r, 98.80.Jk

1. Introduction

In Ref. 1, an analysis of modified gravity theories, which takes in account current CMB data, was presented. As it is stated in this paper: "Those models which are close to ΛCDM are in broad agreement with current constraints on the background

cosmology, but the perturbations may still evolve differently and hence it is important to test their predictions against CMB data." In agreement with these comments, the present paper studies the case of another successfully modified gravity theory that is close to the ΛCDM model.

Any vector-tensor gravity (VTG) theory involves the metric tensor $g^{\mu\nu}$ and a vector field A^{μ}. These fields are coupled to build up an appropriate action leading to the basic equations via variational calculations.

There are many actions and VTG theories,[2,3] here we focus our attention on one of these theories free from quantum ghosts and classical instabilities. It has the same parameterized post-Newtonian limit as general relativity (GR) and may explain cosmic microwave background (CMB) anisotropies as well as GR.[4–7] In this vector-tensor theory, the outer metric corresponding to a spherically symmetric mass distribution has the same form as the well-known Reissner–Nordström solution of Einstein–Maxwell equations,[8] whose source is a charged spherically symmetric mass distribution. This implies that, in the VTG theory (no charges), there are repulsive gravitational forces at stellar scales, just as it occurs in Einstein–Maxwell theory for a charged star. These forces might affect neutron star structure and the gravitational collapse (to be studied elsewhere). Moreover, there is also a gravitational cosmological repulsion, due to the cosmological constant. On account of these facts, this theory shall from now on be called attractive-repulsive vector-tensor gravity (AR-VTG). As it was claimed in Ref. 7, it is convenient to mention that this theory is not a particular case of the Generalized Proca Theories (GPT),[9] which also involve a vector field A^{μ}.

As it was discussed in Ref. 6, the CMB anisotropies produced at $z > 10$ are expected to be identical in GR and AR-VTG; nevertheless, close to $z = 10$, some AR-VTG scalar cosmological modes (see mode definitions in Refs. 10 and 11), involved in the equations describing the evolution of the CMB photon distribution function (see Ref. 12), begin to deviate from those of GR. These deviations might produce significant differences between the CMB anisotropies of GR and AR-VTG, but the redshift dependence of these differences requires numerical estimates which are performed in what follows. Evidently, primary anisotropy is produced at $z \gg 10$ and, consequently, the differences between GR and AR-VTG anisotropies at $z < 10$ must be due to some kind of secondary anisotropy. At these low redshifts, various effects are being produced: (i) the effect due to reionization (hereafter called R-effect), which is due to the interaction of free electrons with CMB photons via Thompson scattering, (ii) the so-called late integrated Sachs–Wolfe (LISW) effect due to large strictly linear scales, and (iii) the Rees–Sciama effect produced by smaller nonlinear scales.

The Rees–Sciama effect is too small to be detected[13]; hence, we focus our attention on the R and the LISW effects.[14,15] In GR, these effects may be estimated with the code CAMB,[16] whereas a new code (hereafter VTCAMB) has been specially designed — by us — to carry out the corresponding estimations in the context of AR-VTG (see Ref. 7).

In this paper, G, a, τ, and z stand for the gravitation constant, the scale factor, the conformal time, and the redshift, respectively. Our signature is $(-,+,+,+)$. Greek indexes run from 0 to 3, while the latin ones from 1 to 3. Symbol ∇ (∂) stands for a covariant (partial) derivative. Whatever the function f may be, $\dot{f}$ stands for the partial derivative with respect to the conformal time. The antisymmetric tensor $F_{\mu\nu}$ is defined by the relation $F_{\mu\nu} = \partial_\mu A_\nu - \partial_\nu A_\mu$. It has nothing to do with the electromagnetic field. Quantities $R_{\mu\nu}$, R, and g are the covariant components of the Ricci tensor, the scalar curvature and the determinant of the matrix $g_{\mu\nu}$ formed by the covariant components of the metric, respectively. Units are chosen in such a way that the speed of light, c, takes on the value $c = 1$. Quantity $\Delta_\ell = \ell(\ell+1)C_\ell/2\pi$, given in $\mu\mathrm{K}^2$, is considered as a measure of CMB angular power spectra. This quantity and other ones depending on it are represented in various figures.

This paper is structured as follows: The AR-VTG theory is summarized in Sec. 2. The origin of the Δ_ℓ deviations between GR and AR-VTG is analyzed in Sec. 3, and the variation of these deviations with the redshift is studied in Sec. 4. Finally, Sec. 5 displays our main conclusions and an appropriate discussion.

2. AR-VTG Foundations

2.1. *Generalities*

AR-VTG is particular parameterization of the general unconstrained VTG proposed by Will, Nordtvedt and Hellings[17,18] in early 1970s. All these theories were based on the action[2]:

$$I = \frac{1}{16\pi G}\int (R + \omega A_\mu A^\mu R + \eta R_{\mu\nu}A^\mu A^\nu - \varepsilon F_{\mu\nu}F^{\mu\nu} + \gamma\nabla_\nu A_\mu \nabla^\nu A^\mu + L_m)\sqrt{-g}d^4x, \tag{1}$$

where ω, η, ε and γ are arbitrary parameters and L_m is the matter Lagrangian density, which couples matter with the fields of the VTG theory.

There is a detailed analysis of the viability for VTGs theories in Ref. 19 which determines the theories that may deserve our attention. This studio includes the calculation of the propagation speeds for the different perturbation modes and also the conditions for the absence of quantum ghosts. Regarding Ref. 19, the parameterization $\omega = 0$, $\eta = \gamma$, leaving ε arbitrary is a viable set of theories in terms of classical stability, local gravity constraints and absence of ghosts. Moreover, the perturbations of mentioned model propagate at the speed of light which leads to the absence of classical unstable modes. AR-VTG theory is obtained when previous parameterization settings are applied to the general unconstrained VTG.

Let us now briefly summarize the AR-VTG basic equations, which were derived in Refs. 4 and 5 from an appropriated action, which is a particularization of the

general vector-tensor action given in Ref. 2. The resulting field equations are

$$G^{\mu\nu} = 8\pi G(T^{\mu\nu}_{\rm GR} + T^{\mu\nu}_{\rm VT}), \tag{2}$$

$$2(2\varepsilon - \gamma)\nabla^{\nu}F_{\mu\nu} = J^{A}_{\mu}, \tag{3}$$

where $G^{\mu\nu}$ is the Einstein tensor, $T^{\mu\nu}_{\rm GR}$ is the GR energy momentum tensor, $J^{A}_{\mu} \equiv -2\gamma\nabla_{\mu}(\nabla\cdot A)$ with $\nabla\cdot A = \nabla_{\mu}A^{\mu}$, and

$$T^{\mu\nu}_{\rm VT} = 2(2\varepsilon-\gamma)\left[F^{\mu}{}_{\alpha}F^{\nu\alpha} - \frac{1}{4}g^{\mu\nu}F_{\alpha\beta}F^{\alpha\beta}\right] - 2\gamma\left[\left\{A^{\alpha}\nabla_{\alpha}(\nabla\cdot A) + \frac{1}{2}(\nabla\cdot A)^{2}\right\}g^{\mu\nu} - A^{\mu}\nabla^{\nu}(\nabla\cdot A) - A^{\nu}\nabla^{\mu}(\nabla\cdot A)\right]. \tag{4}$$

Equation (3) leads to the following conservation law:

$$\nabla^{\mu}J^{A}_{\mu} = 0 \tag{5}$$

for the fictitious current J^{A}_{μ}. Moreover, the conservation laws $\nabla_{\mu}T^{\mu\nu}_{\rm GR} = 0$ and $\nabla_{\mu}T^{\mu\nu}_{\rm VT} = 0$ are satisfied by any solution of Eqs. (2) and (3).

The pair of parameters (ε, γ) must satisfy the inequality $2\varepsilon - \gamma > 0$ to prevent the existence of quantum ghosts and unstable modes in AR-VTG (see Ref. 19).

2.2. *The background cosmology*

Let us now consider a flat uncharged homogeneous and isotropic background universe with matter and radiation where the isentropic uncharged perfect fluid is characterized by an energy density ρ_B and a pressure p_B (subscript B refers to background quantities). In this flat background using conformal time, the metric can be written in the form

$$ds^2 = a^2(\tau)[-d\tau^2 + dr^2 + r^2d\theta^2 + r^2\sin^2\theta d\phi^2]. \tag{6}$$

Furthermore, the covariant components of the vector field are $(A_{0B}(\tau), 0, 0, 0)$ and tensor $F_{\mu\nu}$ vanish. On the other hand, it is worthwhile to notice that the relation $\nabla_{\mu}T^{\mu\nu}_{\rm VT} = 0$ is satisfied (see Ref. 2) so matter and radiation evolve as in the standard Friedmann–Robertson–Walker model of GR (immediately $\nabla_{\mu}T^{\mu\nu}_{\rm GR} = 0$ is obtained).

Taking into account $F_{\mu\nu} = 0$, Eq. (3) leads to

$$J^{A}_{\mu} \equiv -2\gamma\nabla_{\mu}(\nabla\cdot A) = 0, \tag{7}$$

and then the quantity $(\nabla\cdot A)_B$ is a constant and, consequently, tensor $T^{\rm VT}_{\mu\nu}$ has the same form as the energy–momentum tensor corresponding to vacuum; namely, one has $T^{\rm VT}_{\mu\nu} = -\rho^{\rm VT}_{B}g_{\mu\nu}$, where $\rho^{\rm VT}_{B} = \frac{\gamma}{2}(\nabla\cdot A)^2_B = \text{constant} \neq 0$ is the energy density

due to the vector field. This means that the resulting theory is equivalent to GR plus a cosmological constant. In terms of the component $A_{0B}(\tau)$ the Eq. (7) is

$$\ddot{A}_{0B} + 2A_{0B}\left(\frac{\ddot{a}}{a} - 3\frac{\dot{a}^2}{a^2}\right) = 0, \tag{8}$$

while Eq. (2) is

$$3\frac{\dot{a}^2}{a^2} = 8\pi G a^2(\rho_B + \rho_B^{\mathrm{VT}}) \tag{9}$$

and

$$-2\frac{\ddot{a}}{a} + \frac{\dot{a}^2}{a^2} = 8\pi G a^2(p_B + p_B^{\mathrm{VT}}), \tag{10}$$

where

$$\rho_B^{\mathrm{VT}} = -p_B^{\mathrm{VT}} = \frac{1}{2}\gamma(\nabla\cdot A)_B^2 = \frac{\gamma}{2a^4}\left(\dot{A}_{0B} + 2\frac{\dot{a}}{a}A_{0B}\right)^2. \tag{11}$$

Hence, the equation-of-state is $w^{\mathrm{VT}} \equiv p^{\mathrm{VT}}/\rho^{\mathrm{VT}} = -1$, so as the energy density of the evolving field is constant, we can state that this field acts as a cosmological constant. Obviously, the condition $\gamma > 0$ must be required to have a positive A^μ energy density in the background universe (see Ref. 6); hence, taking into account the previous inequality $2\varepsilon - \gamma > 0$, the inequalities $\varepsilon > \frac{\gamma}{2} > 0$ must be satisfied.

The necessary initial values for the integration are obtained at high redshift ($z_{\mathrm{in}} \sim 10^8$) during the radiation dominated era, where it is found that $a \propto \tau$ and $A_{0B}(\tau) \propto \tau^3$ satisfy the above background field equations. At $z = z_{\mathrm{in}}$, one finds

$$\tau_{\mathrm{in}} = \left(\frac{\dot{a}}{a}\right)_{\mathrm{in}}^{-1}, \quad (A_{0B})_{\mathrm{in}} = -\frac{(\nabla\cdot A)_B}{5(1+z_{\mathrm{in}})}\left(\frac{\dot{a}}{a}\right)_{\mathrm{in}}^{-1}, \tag{12}$$

where subscript "in" of previous quantities refers to initial values at $z = z_{\mathrm{in}}$.

2.3. *The cosmological perturbations*

In order to describe cosmological perturbations, the formalism summarized in Ref. 10 (see also Ref. 11) is used. In this formalism, there are three types of perturbations whose evolution is independent during the linear regime: scalar, vector, and tensor fluctuations. There are no tensor modes involved in the expansion of the introduced vector field, so the existing ones satisfy the same equations as in GR. Formally, the vector fluctuations are as in Einstein–Maxwell equations. The main reason lies in the fact that the action (1) is full equivalent to

$$I = \frac{1}{16\pi G}\int\left[R + \left(\frac{1}{2}\gamma - \varepsilon\right)F_{\mu\nu}F^{\mu\nu} + \gamma(\nabla\cdot A)^2 + L_m\right]\sqrt{-g}d^4x \tag{13}$$

for the parameterization $\omega = 0$, $\eta = \gamma$, and this action differs in essence, from the Einstein–Maxwell one, in the term proportional to $(\nabla\cdot A)^2$, which is a scalar.

At linear level, the vector perturbation of the vector field can be written $A^{(1)}_{\mu} = (0, A^{(1)}Q^{(1)}_i)$, where $Q^{(1)}_i$ are the vector harmonics which are a solution of the Helmholtz equation $\nabla^2 Q^{(1)}_i = -k^2 Q^{(1)}_i$ (see Ref. 10), and k is the wave number that sets the spatial scale of the perturbation. The evolution equation for the vector modes amplitude $A^{(1)}$ is[7]

$$\ddot{A}^{(1)} + k^2 A^{(1)} = 0. \tag{14}$$

It is interesting to realize that this mode is uncoupled from the rest of mode equations, so it has no impact on the evolution of the other modes.

Finally, all the scalar modes of GR are also involved in AR-VTG but, in order to describe the scalar modes associated to the field A_{μ}, we introduce a new gauge invariant scalar mode[5,6] $(\nabla \cdot A)^{(0)}$ which is the first-order term in the harmonic expansion of the scalar function $(\nabla \cdot A)$ defined as follows:

$$(\nabla \cdot A) = (\nabla \cdot A)_B + (\nabla \cdot A)^{(0)} Q^{(0)}, \tag{15}$$

where the scalar harmonic $Q^{(0)}$ is a solution of the Helmholtz equation $\nabla^2 Q^{(0)} = -k^2 Q^{(0)}$ (see Ref. 10). There are no more independent AR-VTG scalar modes. From Eq. (7), the following uncoupled differential equation for the new mode is obtained:

$$(\nabla \cdot A)^{(0)\bullet\bullet} + 2aH(\nabla \cdot A)^{(0)\bullet} + k^2(\nabla \cdot A)^{(0)} = 0. \tag{16}$$

This equation just involves, apart from the new AR-VTG scalar mode and its derivatives, the background functions $a(\tau)$, $H(\tau) \equiv \dot{a}/a^2$ and the wave number. It is convenient to write scalar perturbation equations in the synchronous gauge and in terms of the scalar modes defined in Ref. 12, the reason is because those are the functions and gauge used by the original CAMB code and the modified one VTCAMB. There are just AR-VTG corrections terms to the standard GR in equations (21a)–(21c) derived in Ref. 12, this set of modified equations are as follows:

$$k^2\tilde{\eta} - \frac{1}{2}aH\dot{\tilde{h}} = -4\pi G[a^2\rho_B\tilde{\delta} + \Psi^{(0)}_A], \tag{17}$$

$$k^2\dot{\tilde{\eta}} = 4\pi G\left[a^2(\rho_B + p_B)\tilde{\theta} + \frac{\gamma}{8\pi G}k^2 A_{0B}(\nabla \cdot A)^{(0)}\right], \tag{18}$$

$$\ddot{\tilde{h}} + 2aH\dot{\tilde{h}} - 2k^2\tilde{\eta} = -24\pi G[a^2 p_B\pi_L - \Psi^{(0)}_A], \tag{19}$$

where $\Psi^{(0)}_A \equiv -\frac{\gamma}{8\pi G}[a^2(\nabla \cdot A)_B(\nabla \cdot A)^{(0)} + A_{0B}(\nabla \cdot A)^{(0)\bullet}]$. In the above equations, $\tilde{\eta}$ and $\tilde{h}$ are the scalar modes related with the metric, while $\tilde{\delta}$, $\tilde{\theta}$ and π_L are the scalar modes related with fluid (density fluctuation, divergence of fluid velocity and the isotropic pressure perturbation, respectively). The same functions (without the tilde) and its definitions are found in Ref. 12, while the π_L one can be located in Ref. 10. The rest of scalar modes equations remain unaltered (see Eqs. (92) and subsequent in paper Ref. 12).

As in previous subsection, initial conditions equations for the AR-VTG scalar modes at redshift ($z_{\rm in} \sim 10^8$) in the radiation dominated era are obtained. In GR, the initial conditions equations involve a normalization constant named C at Ref. 12 while in AR-VTG it involves an extra one we call D, that is related with the initial spectrum of the new scalar mode in the following manner: $(\nabla \cdot A)^{(0)} = Dk^4$. The complete set of modified initial conditions equations can be found in Ref. 7 labeled as (2.23).

3. CMB Anisotropy Differences Between GR and AR-VTG

3.1. *Numerical computational fitting*

In order to fit observational data with the model predictions an adapted and modified version of the standard well-known codes COSMOMC[20] (hereafter VTCOSMOMC) and CAMB have been used. There are a lot of tasks related with the adaptation and modifications of the codes as the inclusion of the background and scalar modes extra field equations, and its corresponding initial conditions equations, the modification of the scalar modes equations including the new terms and again its modified corresponding initial conditions equations. But this is not enough, the introduction of the new parameter implies changes at original COSMOMC (the Markov sample chains generator software) code, modifications related with the integration steps in wave number k and in time, numerical issues and other technical concerns.

As related in the above subsection, there is a new constant D whose absolute value $|D|$ normalizes the spectrum of the vector field A_μ (its divergence) scalar cosmological perturbations. This is the new parameter that has been added in the different fitting calculations. Apart from the mentioned above, we include six GR parameters to conform a minimal base model to fit, those parameters are: $\Omega_b h^2$, $\Omega_{\rm DM} h^2$, τ_{re}, n_s, $\log[10^{10} A_s]$, and θ, where Ω_b and $\Omega_{\rm DM}$ are the density parameters of baryons and dark matter, respectively, h is the reduced Hubble constant, τ_{re} is the reionization optical depth, n_s is the spectral index of the power spectrum of scalar modes, and A_s is the normalization constant of the same spectrum whose form is $P(k) = A_s k^{n_s}$, finally, the parameter θ (angular acoustic scale) is defined by the relation $\theta \times 10^{-2} = r_s(z_*)/d_A(z_*)$, where $r_s(z_*)$ is the sound horizon at decoupling redshift z_*, and $d_A(z_*)$ is the angular diameter distance at the same redshift. This minimal base model is expanded for some cases when tensor modes are included, in such a case, following additional parameters are considered: $r_{0.05}$ (the primordial tensor to scalar initial amplitude at the pivot scale of $k_0 = 0.05\,{\rm Mpc}^{-1}$), and $dn_s/d\ln k$ (running index).

A varied combination of evidence sources that includes Ia supernovae (SNIa), WMAP 7 years CMB anisotropies (WP7), Planck CMB anisotropies (Planck), WMAP polarization anisotropy at low $\ell \lesssim 23$ (WP), baryon acoustic oscillations (BAO) have been used. A complete analysis of the results can be found at Refs. 6 and 7, however, let us summarize useful obtained information for the current studio.

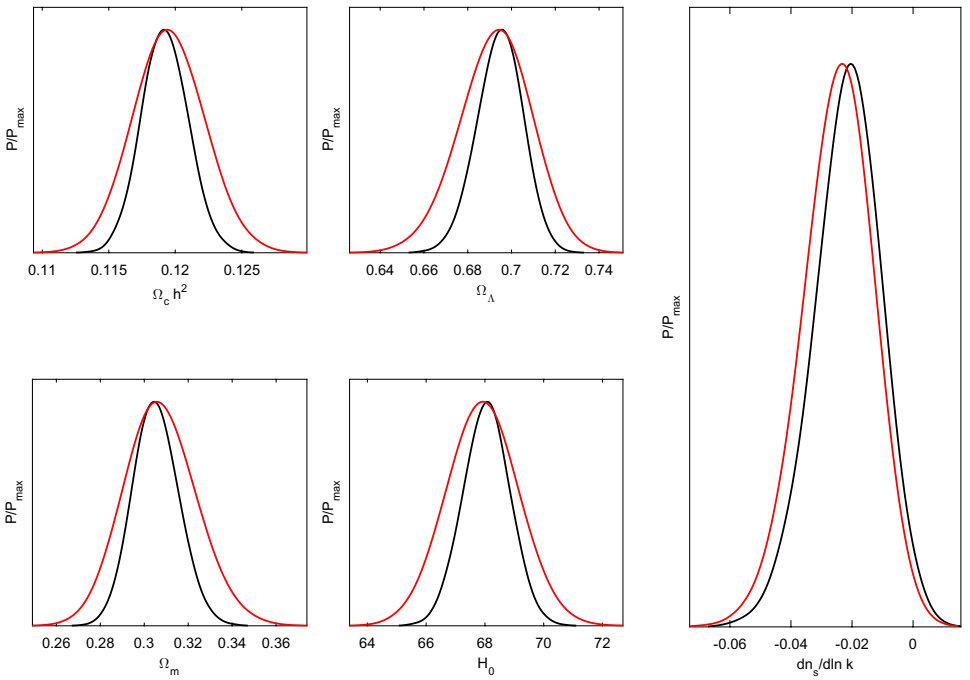

Fig. 1. (Color online) Five panels representing the normalized to unity ($P/P_{\max}$) marginalized likelihood function for different standard GR parameters; Ω_m is the density parameter of matter and H_0 is the Hubble constant parameter. Black color represents the function for GR while the red one is used for AR-VTG.

When the constant D is considered as an additional parameter to be adjusted and a certain confidence level is assumed, we have found that, in AR-VTG fitting calculations, most GR parameters belong to intervals wider than those of the GR fitting calculations and, consistently, quantity $|D|$ takes on nonvanishing values. As a sample, see Fig. 1 where the left four panels represent the normalized likelihood for different standard GR parameters (the best fit values, including the 68% confidence intervals can be found in Table 1); at the stretched right panel the

Table 1. Minimal fit for 6 (GR) + 1 (D) parameters in the AR-VTG model. The evidence sources used are Planck CMB anisotropies and WMAP polarization anisotropy at low $\ell \lesssim 23$.

Parameter	Best fit	68% Lower limit	68% Upper limit
$D \times 10^{-8}$	1.596	−2.149	2.149
$\Omega_b h^2$	0.02216	0.02179	0.02235
$\Omega_{\rm DM} h^2$	0.1187	0.1169	0.1222
τ_{re}	0.0893	0.0749	0.1013
n_s	0.9657	0.9535	0.9684
$\log[10^{10} A_s]$	3.085	3.060	3.110
θ	1.0411	1.0407	1.0419

normalized likelihood function for the running index parameter, when tensor modes are included, is presented. This is a pattern that is repeated when using different evidence data sources combinations and strongly suggests that a parameter $D \neq 0$ facilitates the adjustments between predictions and cosmological observations.

Parameter $|D|$ plays a positive statistical role in the study of AR-VTG scalar perturbations. Depending on the set of evidence sources considered and the inclusion or not of tensor fluctuations (and the parameters related with it), different intervals for the confidence level of 1σ (68%), 2σ (95%), and 3σ (99.7%) are achieved. Figure 2 represents a summary of mentioned results, for instance, at 2σ confidence level those are: $[-3.876,\ 3.876]$ for just scalar perturbations and Planck + WP, $[-4.005,\ 4.005]$ same as previous one but including BAO, and $[-5.442,\ 5.442]$ when including tensor modes with running index and using Planck + WP as evidence sources.

3.2. *On the CMB anisotropy differences*

Let us now describe the method used to analyze the origin of the CMB anisotropy differences between GR and AR-VTG.

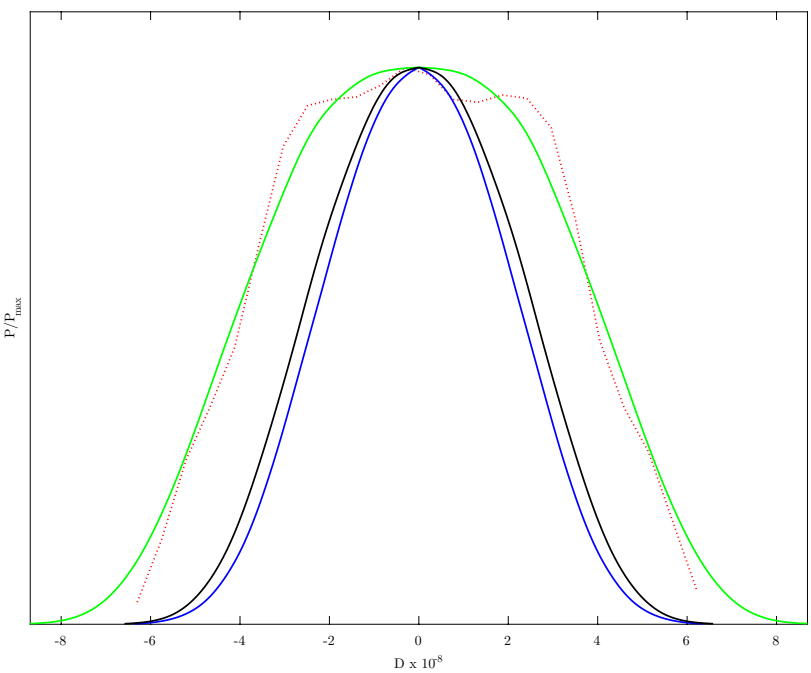

Fig. 2. (Color online) Marginalized distribution functions normalized to unity for the parameter $D \times 10^{-8}$ in various fits. The dotted red curve was built with WMAP and SNIa data whereas blue solid, black, and green lines provide $(P/P_{\max})$ use Planck + WP just with scalar modes, Planck + WP including tensor modes without running index, and Planck + WP including tensor modes and running index, respectively.

Codes CAMB and VTCAMB are used to estimate the R and LISW effects at $z \leq 10$. Reionization is modeled by using the standard optical depth τ_{re} parameter.

In any case, results from CAMB based on a minimal six parameters fit model are compared with the results obtained with VTCAMB for the same values of the six parameters plus a new parameter characteristic of AR-VTG. This parameter labeled D will take on the value 4×10^8, which was proved to be compatible with CMB observations at the 2σ confidence level (see previous subsection and Ref. 7).

We use two sets of six parameters obtained in previous papers — in the context of GR — to fit theoretical predictions and observations. These sets are hereafter called ΛCDM-2013 and ΛCDM-2015. The six parameter values for ΛCDM-2013 (ΛCDM-2015) are given in the first (second) data row of Table 2.

Five of the six parameters given by CAMB — in the GR context — take on similar values whatever the observational data may be (WMAP, PLANCK, and so on); however, parameter τ_{re} depends on the CMB polarization data used in fit calculations. The ΛCDM-2013 parameter values — obtained in Ref. 7 — were derived by using Planck data about the CMB temperature distribution, plus WMAP data on CMB polarization anisotropy at low $\ell \lesssim 23$, and the resulting τ_{re} is close to 0.093 (first data row of Table 2); nevertheless, the ΛCDM-2015 parameter values, given in the second data row of Table 2, were derived in Ref. 21 by using both temperature and polarization Planck data (see column 3 of Table 4 in this last reference); in this second case, the parameter value τ_{re} is close to 0.067; namely, this parameter is rather smaller than that of the ΛCDM-2013 fit, which is a consequence of important differences in the polarization data. Both fits have been performed by using CAMB and COSMOMC codes. December 2013 (November 2015) versions were used to get the ΛCDM-2013 (ΛCDM-2015) parameter values.

As it has been stated in Sec. 1, the differences between the CMB anisotropies of GR and AR-VTG must be due to a combination of the R and LISW effects at $z \leq 10$. Reionization contributes to the LISW effect[14] ($R1$-effect) and, moreover, it also creates anisotropy due to path mixing, Doppler effects due to motions in the reionization electron distribution, and so on ($R2$-effect). Our main goal is to disentangle the $R1$, $R2$, and LISW contributions to find out the nature of the aforementioned differences. Since there are well defined terms giving the LISW effect — in CAMB and VTCAMB — and these terms include reionization contributions ($R1$-effect), we can proceed as follows:

(i) Once a data row of Table 2 has been selected and the value $D = 4 \times 10^8$ has been fixed, Codes CAMB and VTCAMB may be used to calculate the total Δ_ℓ numbers in GR and AR-VTG, respectively.

Table 2. Two minimal fits (six parameters) in the standard ΛCDM model.

Parameters	$\Omega_b h^2$	$\Omega_{\rm DM} h^2$	τ_{re}	n_s	$\log[10^{10} A_s]$	θ
ΛCDM-2013	0.02209	0.1195	0.0927	0.9633	3.093	1.0415
ΛCDM-2015	0.02227	0.1184	0.067	0.9681	3.064	1.04106

(ii) For the same parameters, the LISW contribution to the Δ_ℓ quantities may be easily calculated. This computation may be performed by integrating, from redshift 10 to 0, only the terms giving the LISW effect (including $R1$); namely, by canceling any other contribution to the CMB angular power spectrum, including $R2$ reionization effects (not contained in LISW); in this way, only the reionization contribution, $R1$, to the LISW effect is taken into account.

Results obtained with this procedure may be used to calculate, for the chosen parameters, both absolute and relative deviations between the GR and AR-VTG angular power spectra. These deviations may be estimated for the total Δ_ℓ quantities, and also for the LISW contribution to the angular power spectrum. The absolute deviations are $\delta_\ell^{\rm abs} = |\Delta_\ell({\rm GR}) - \Delta_\ell({\rm AR\text{-}VTG})|$, whereas the relative ones are $\delta_\ell^{\rm rel} = 2[|\Delta_\ell({\rm GR}) - \Delta_\ell({\rm AR\text{-}VTG})|]/[\Delta_\ell({\rm GR}) + \Delta_\ell({\rm AR\text{-}VTG})]$. These deviations are presented in Figs. 3 to 6.

The top panels of Fig. 3 exhibit the total Δ_ℓ quantities obtained from the parameters of the first (ΛCDM-2013, left) and second (ΛCDM-2015, right) rows of Table 2. In these panels, solid (dotted) lines correspond to GR (AR-VTG theory with $D = 4 \times 10^8$). From the comparison of solid and dashed lines, it follows that for $D = 4 \times 10^8$ there are deviations from GR in the ℓ interval represented. For $\ell > 60$, both theories lead to almost the same angular power spectrum. The relative

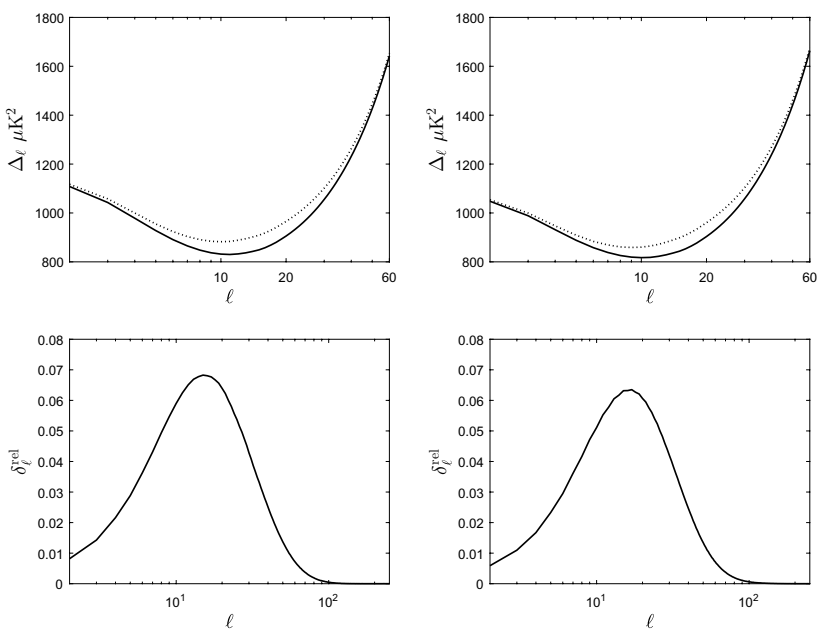

Fig. 3. Top left (right) panel shows the total CMB angular power spectrum Δ_ℓ for ΛCDM-2013 (ΛCDM-2015) parameters. In these panels, solid (dotted) line corresponds to the ΛCDM model of GR (AR-VTG with $D = 4 \times 10^8$). Bottom panels present the relative deviations, $\delta_\ell^{\rm rel}$, between GR and AR-VTG, for the pairs of curves displayed in the top panels located at the same column.

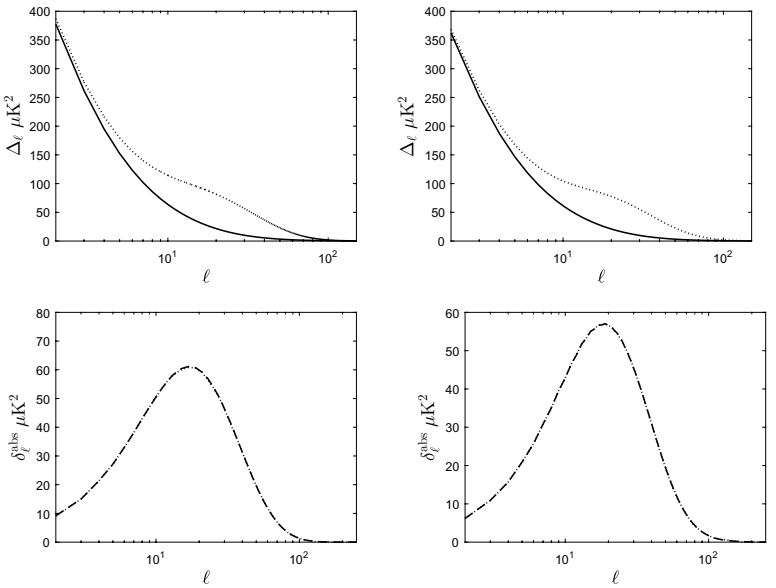

Fig. 4. Top panels are as those of Fig. 3, but Δ_ℓ is here the LISW contribution to the total CMB angular power spectra. In bottom panels, the dashed (dotted) line displays the absolute deviations, $\delta_\ell^{\rm abs}$, between GR and AR-VTG, for the pairs of curves shown inside the top panel located in the same column of this figure (of Fig. 3).

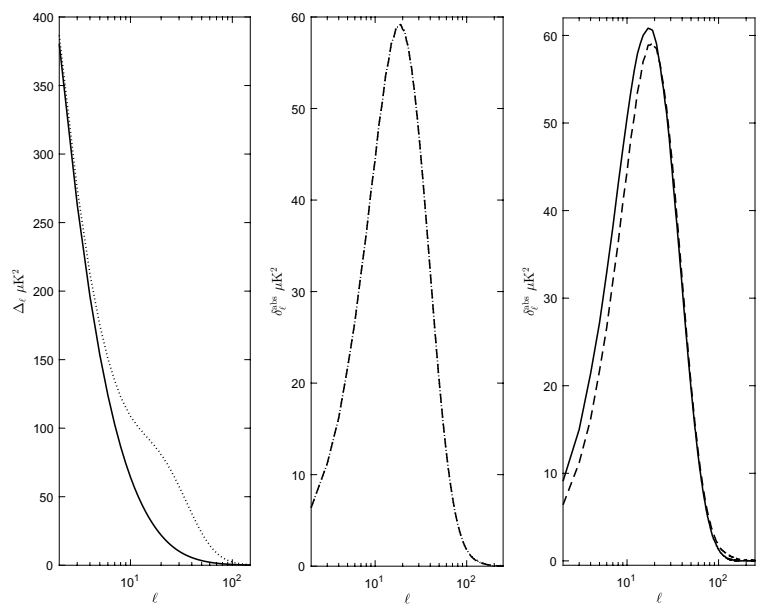

Fig. 5. Left and central panels have the same structure as the left top and left bottom panels of Fig. 4. In the panels of this figure, quantities Δ_ℓ and $\delta^{\rm abs}$ have been calculated in the absence of reionization. In the right panel, solid (dashed) line gives LISW absolute deviations, $\delta^{\rm abs}$, between GR and AR-VTG with (without) reionization. All the curves correspond to the case ΛCDM-2013.

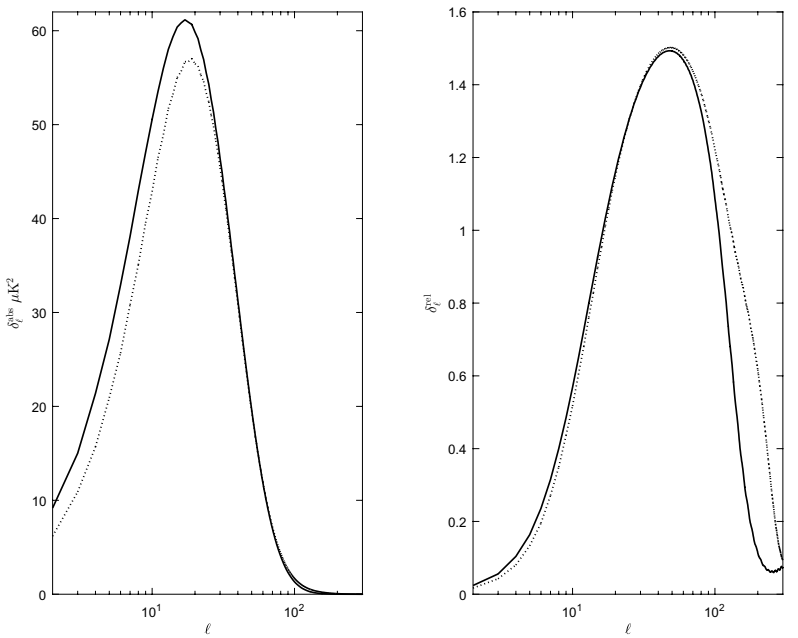

Fig. 6. Left (right) panel shows absolute (relative) LISW deviations between GR and AR-VTG. Solid (dotted) lines correspond to ΛCDM-2013 (ΛCDM-2015).

deviations are given in the bottom panels, where it can be seen that the values of these deviations are close to 0.06 (6%) for ℓ values in the interval $(10, 20)$, being greater than 0.01 (1%) between $\ell = 2$ and $\ell = 60$. We will not discuss the importance of these deviations, as it was already done in previous papers[6,7] from the statistical point of view. We are only interested in the nature of these deviations, which are not either negligible or too large for the chosen D value. The key question now is: what kind of effect produces the relative deviations represented in Fig. 3? To answer this question, we use Figs. 4 and 5. We have to emphasize that these two figures also reveal to us that, while the aforementioned relative deviations in the ℓ interval are around 6%, when the isolated contribution due to LISW is considered, those deviations reach, and even exceed, 100%.

If the absolute deviations corresponding to the total Δ_ℓ quantities and those of the LISW contribution (including $R1$) may be considered the same; namely, if the differences among these two absolute deviations are smaller than the numerical errors in the C_ℓ coefficients due to CAMB and VTCAMB, it can be stated that the total deviations between GR and AR-VTG are fully due to the LISW effect; however, if these differences are greater than the expected numerical errors, a part of the total deviations between GR and AR-VTG would be due to reionization through effects which are not included in the total LISW ($R1$).

Each of the top panels of Fig. 4 has the same structure as the corresponding top panel of Fig. 3; only the displayed quantities are different in these figures: the total

Δ_ℓ coefficients in Fig. 3 and the contribution due to the LISW in Fig. 4. In the bottom panels of this last figure, there are two lines, the dashed line gives the absolute differences between GR and AR-VTG corresponding to the total C_ℓ coefficients represented in the top panels of Fig. 3, whereas the dotted line displays the absolute differences of the LISW contributions given in the top panels of Fig. 4. The coincidence of these lines, which are indistinguishable to the eye, suggests that the total deviations between GR and AR-VTG are essentially due to the LISW effect (see previous paragraph). See also Sec. 5 for a detailed measurement of the relative deviations between the dotted and dashed lines of the bottom panels.

Let us now repeat our estimations of the total Δ_ℓ quantities and the LISW contributions to them in the absence of reionization. For the sake of briefness, only the results corresponding to ΛCDM-2013 parameters (first data row of Table 2) are presented. Similar results have been verified for ΛCDM-2015 parameters (second data row of Table 2). Since only the LISW effect produces CMB anisotropy at $z < 10$, the total and LISW absolute deviations between GR and AR-VTG must coincide. This fact has been verified and results are presented in Fig. 5. Left and central panels of this figure have the same structure as top left and bottom left panels of Fig. 4. The two curves of the central panel are almost identical (see Sec. 5 for measurements of deviations), which confirms that the total anisotropy is a LISW effect. Right panel shows LISW absolute deviations between GR and AR-VTG with and without reionization. It is evident that reionization affects the LISW absolute deviations (R1-effect), but the absolute deviations of the total C_ℓ quantities are affected in such a way that the two curves of the bottom left panel of Fig. 4 (with reionization) are very similar, and those of the central panel of Fig. 5 (without reionization) are also almost identical.

Figure 6 shows absolute (left) and relative (right) differences between GR and AR-VTG for the LISW contributions to Δ_ℓ. Solid lines (ΛCDM-2013 parameters) and dotted lines (ΛCDM-2015) do not coincide. A remarkable difference appears in both cases since reionization is very different for ΛCDM-2013 and ΛCDM-2015 parameters (see the values of parameter τ_{re} in Table 2). In spite of this fact, the total Δ_ℓ quantities are also different for ΛCDM-2013 and ΛCDM-2015 and, as it may be appreciated in the two bottom panels of Fig. 4, where the dotted and dashed curves almost coincide for ΛCDM-2013 (left) and also for ΛCDM-2015 (right), which strongly suggests that — whatever the fit parameters may be — total deviations are due to the LISW effect at $z < 10$.

3.3. *The LISW in the best fit models*

Once the nature of the deviations between RG and AR-VTG, and how these differences are generated in terms of redshift have been presented, it is interesting to compare the LISW anisotropies predictions between best fit models.

So now, instead of using the parameter set values of a LCDM best fit model to be compared with an AR-VTG model that is built from the first one, that is, uses

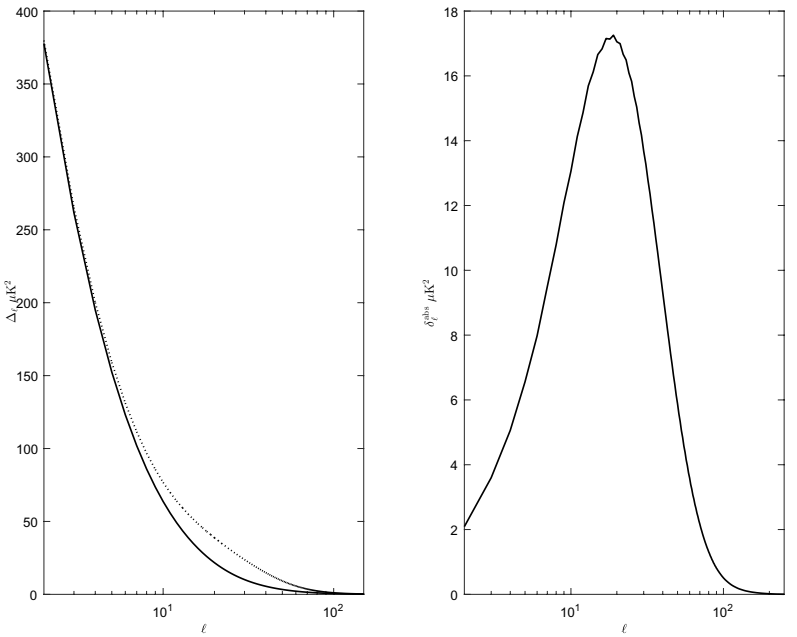

Fig. 7. Presented panels as are those like left and middle in Fig. 5, but the parameter values correspond to the LCDM-2013 model presented at first row of Table 2 for the solid line, while for the dotted line, the parameters values are those located in Table 1 for the AR-VTG fit.

the mentioned parameter set values of the LCDM best fit model, plus a reasonable value for the characteristic AR-VTG parameter (D parameter), the two models to be used are: the LCDM-2013 minimal fit (see first row of Table 2) and the AR-VTG best fit model presented in Table 1.

The results of the predictions of the LISW contribution to the CMB anisotropies, of the aforementioned models, are presented in Fig. 7. As in previous comparisons, the maximum absolute differences are reached in the range of ℓ $(10, 20)$, this time those relative deviations are $\sim 50\%$ when examining just the LISW contributions, however, when the total CMB anisotropies are considered, those maximums are between $\sim 1\%$ and $\sim 2\%$. It has been described in Sec. 3.1 that a set of different results have been obtained when different evidences, sources and extended models are studied (see Refs. 6 and 7 for details). In this global context, we can affirm that the total CMB anisotropies differences reach a maximum between $\sim 2\%$ and $\sim 5\%$. If we also take into account that, except in the particular case of considering tensor modes and running index, the best fit values obtained for the common parameters of GR and AR-VTG models are very similar, we may conclude that a reasonable doubt exists as to whether CMB has enough discriminating character. Another important issue to take into account is the fact that the low values ℓ of the CMB are mainly affected by cosmic variance. In such a case additional cross-correlation tests might be useful.

The cross-correlation between CMB and some tracers of large scale structure surveys (LSS) was first proposed by Crittenden and Turok (see Ref. 22), allowing us to isolate the LISW anisotropy contribution. These cross-correlations and certain statistical estimators have been successfully used to provide a physical evidence for dark energy,[23] to derive constraints on the dark energy[24,25] or neutrino masses,[26] to detect coupling between dark energy and dark matter at low redshifts,[27] and other issues. But also provides a mechanism for differentiating dark energy from a modified gravity, even for an identical background expansion[28,29] which is the case we are dealing with.

Although a complete study, based on new cross-correlations, is out of the scope of the current paper, we will present below some preliminary results in this regard. With this aim, next we will compare some cross-correlations theoretical predictions for GR and AR-VTG, and for that purpose, let us first introduce and define some suitable useful concepts.

The temperature fluctuation due to the LISW effect in a certain direction $\hat{n}_1$ is provided by the expression

$$\frac{\Delta T}{T}(\hat{n}_1) = -2 \int e^{-\tau_{re}(z)} \frac{d\Phi}{dz}(\hat{n}_1, z) dz, \tag{20}$$

where $e^{-\tau_{re}(z)}$ is the visibility function of the photons, and Φ is the gravitational potential in the Newtonian gauge. The observed density contrast for a certain direction $\hat{n}_2$ is given by

$$\delta_g(\hat{n}_2) = \int b_g(z) \frac{dN}{dz}(z) \delta_m(\hat{n}_2, z) dz, \tag{21}$$

where $b_g(z)$ is the galaxy bias, dN/dz is the selection function of the survey, and δ_m is the matter density fluctuation. For a certain map of CMB anisotropies and a survey of galaxies, the cross-correlation and the auto-correlation function are defined as

$$C^{Tg}(\theta) \equiv \left\langle \frac{\Delta T}{T}(\hat{n}_1) \delta_g(\hat{n}_2) \right\rangle, \tag{22}$$

and

$$C^{gg}(\theta) \equiv \langle \delta_g(\hat{n}_1) \delta_g(\hat{n}_2) \rangle, \tag{23}$$

with the average, denoted by the angular brackets, carried over all the pairs at the equal angular distance $\theta = |\hat{n}_1 - \hat{n}_2|$. For computing purposes, we decompose these quantities using the Legendre polynomials P_ℓ as

$$C^{Tg}(\theta) = \sum_{\ell=2}^{\infty} \frac{2\ell + 1}{4\pi} C_\ell^{Tg} P_\ell[\cos(\theta)], \tag{24}$$

the cross-correlation and the autocorrelation power spectra are obtained from

$$C_\ell^{Tg} = 4\pi \int \frac{dk}{k} \Delta^2(k) I_\ell^{\mathrm{ISW}}(k) I_\ell^g(k), \tag{25}$$

and

$$C_\ell^{gg} = 4\pi \int \frac{dk}{k} \Delta^2(k) I_\ell^g(k) I_\ell^g(k), \tag{26}$$

respectively. The function $\Delta(k)$ is the matter power spectrum, and the two integrals functions $I_\ell^{\rm ISW}$ and $I_\ell^{\rm ISW}$ are defined as follows:

$$I_\ell^{\rm ISW} = -2 \int e^{-\tau_{re}(z)} \frac{d\Phi_k}{dz} j_\ell[kr(z)] dz, \tag{27}$$

and

$$I_\ell^g = \int b_g(z) \frac{dN}{dz}(z) \delta_m^k(z) j_\ell[kr(z)] dz, \tag{28}$$

where Φ_k, δ_m^k are the Fourier components of the gravitational potential and matter perturbations, respectively, $j_\ell[kr(z)]$ are the spherical Bessel functions and $r(z)$ is the comoving distance at redshift z. In order to compute those related quantities, a new version of the CROSS-CMBFAST,[24] say VTCROSS-CMBFAST, which in turn is an adaptation of the well-known CMBFAST[30] code, is used. In order to go ahead with the calculations, some functions are still needed, these are: the galaxy bias $b_g(z)$, and the selection function of the survey dN/dz. Let us consider a very simple model with $b_g(z) = 1$ and $dN/dz \sim z^2 \exp[-(10z)^{1.5}]$, that is we select a Gaussian distribution for selection function of the survey as in Ref. 24. With this set of options and VTCROSS-CMBFAST, the correlation function $C^{Tg}(\theta)$ is calculated for the models: AR-VTG best fit (see Table 1), ΛCDM-2013 (row 1 in Table 2) and AR-VTG with $D = 4 \times 10^8$ (the model introduced in Sec. 3.2).

The results are represented in Fig. 8. In this figure, one observes that both models are quite similar; there are relative differences of a $\sim 3\%$ located in the

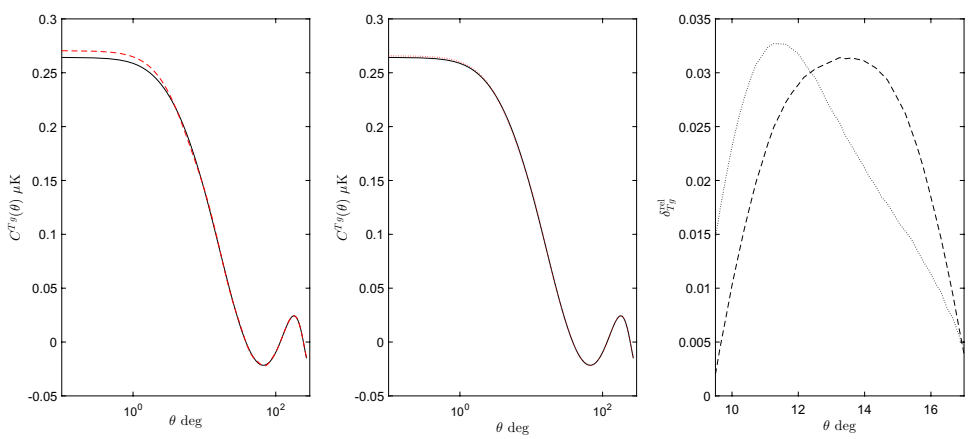

Fig. 8. (Color online) Left (middle) panel represents the $C_{Tg}(\theta)$ correlations, the solid line has been built using the ΛCDM-2013 parameters model while the red dashed (dotted) one corresponds to AR-VTG best fit (AR-VTG with $D = 4 \times 10^8$) settings. In the right panel, dotted (dashed) line provides the relative deviations in the $9 < \theta < 17$ range.

range $9 \lesssim \theta \lesssim 17$, in fact the main contribution to a C_ℓ^{TT} multipole corresponds to $\theta = \pi/\ell$, so it's something that might be expected. This is the corresponding ℓ range where we found (in the previous section) C_ℓ^{TT} deviations between the compared models. The relative differences $\delta_{Tg}^{\rm rel}$ are defined in the same way we did in Sec. 3.2 for $\delta_\ell^{\rm rel}$.

4. On the Generation of Absolute Deviations $\delta_\ell^{\rm abs}$

After analyzing the nature of the differences between the CMB anisotropies in GR and AR-VTG, let us study how these differences are generated between redshifts 10 and 0. To do that, the differences have been estimated while the redshift varies from 10, to 5, 4, 3, 2, 1 and 0. Results are presented in Fig. 9, where each panel corresponds to one of the above redshift variations, which is given above the panel.

For the ΛCDM-2013 parameters, the black dashed lines (ΛCDM model of GR) must be compared with the red dashed lines (AR-VTG with $D = 4\times10^8$). The separation between these lines measures the differences between the CMB anisotropies in GR and AR-VTG. Top left panel shows that, for $10 > z > 5$, these Δ_ℓ differences reach only a few tenths of μK^2, and for $10 > z > 3$ (top right panel) a few μK^2; hence, we can conclude that the differences are essentially generated for $3 > z > 0$. See bottom panels for details.

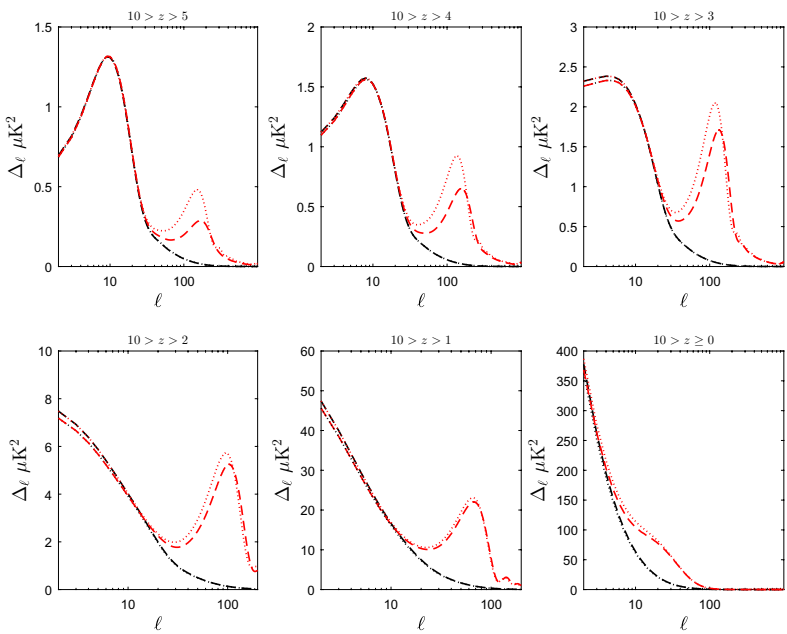

Fig. 9. (Color online) LISW contributions to Δ_ℓ generated in the redshift intervals indicated above the panels. There are two black and two red curves in each panel. Black (red) dashed lines show LISW contributions to Δ_ℓ for ΛCDM-2013 in the ΛCDM model of GR (AR-VTG with $D = 4 \times 10^8$). Same for black and red dotted lines in the ΛCDM-2015 parameter configuration.

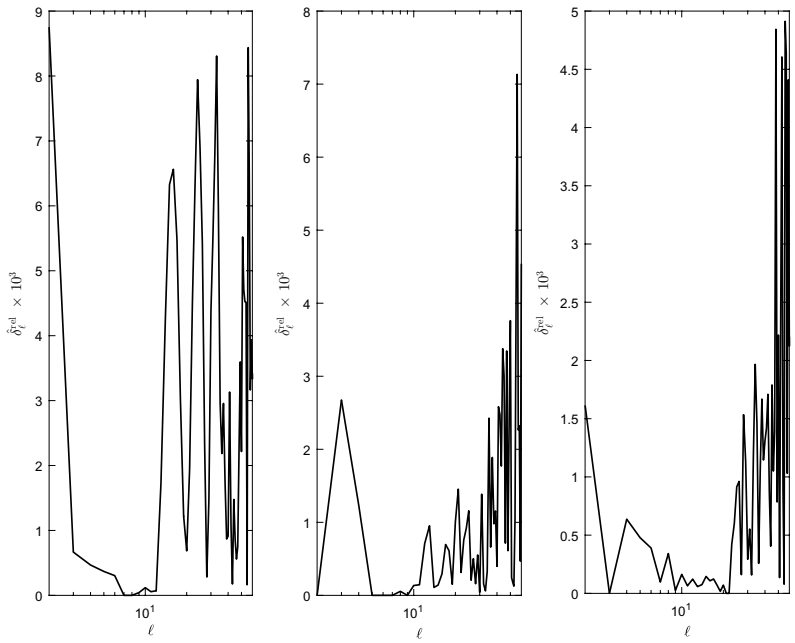

Fig. 10. Representation of the $\hat{\delta}_\ell^{\rm rel}$ quantities in terms of ℓ. Left: for the left bottom panel of Fig. 4. Center: for the central panel of Fig. 5. Right: for the right bottom panel of Fig. 4.

The same may be concluded, for the ΛCDM-2015 parameters, from the comparison between black dotted lines (ΛCDM model of GR) and red dotted lines (AR-VTG with $D = 4 \times 10^8$); hence, the conclusion that the differences between the CMB anisotropies in GR and AR-VTG is mainly generated for $3 > z > 0$, is a robust conclusion almost independent on the selected parameters.

5. Discussion and Conclusions

Our main conclusions are the following: The total absolute Δ_ℓ deviations, between the ΛCDM model of GR and AR-VTG with $D = 4 \times 10^8$, are due to the LISW effect (including $R1$). These deviations are essentially produced between redshifts 3 and 0 with the main part generated for $z \leq 1$. The relative deviations are close to 6% for $10 \leq \ell \leq 20$ and greater than 1% for $2 \leq \ell \leq 60$.

Up to now, the nature of the aforementioned deviations has been suggested by the fact that the dotted and dashed lines of three panels are almost identical to the eye. These three panels are the left bottom panel of Fig. 4 (ΛCDM-2013 parameters with reionization), the central panel of Fig. 5 (ΛCDM-2013 parameters without reionization), and the right bottom panel of Fig. 4 (ΛCDM-2015 parameters with reionization). Let us now prove that the relative differences, $\hat{\delta}_\ell^{\rm rel}$, between the dotted and the dashed lines of each of these three panels are smaller than the relative errors of CAMB and VTCAM calculations, which, based on our hard numerically

computational tests and the settings we fix in terms of a balance between accuracy and performance, may be estimated to be around 1%. These relative differences are $\hat{\delta}_\ell^{\rm rel} = 2[|\delta_\ell^{\rm abs}(\text{dot}) - \delta_\ell^{\rm abs}(\text{dash})|]/[\delta_\ell^{\rm abs}(\text{dot}) + \delta_\ell^{\rm abs}(\text{dash})]$. Quantities $\hat{\delta}_\ell^{\rm rel}$ are given in the three panels of Fig. 10. In any case, these quantities are smaller than 0.001 and, consequently, they are smaller than the numerical errors.

The LISW effect, relevant for $\ell \leq 100$, is produced at low redshifts and, consequently, it may be detected by looking for cross correlations between the CMB temperature distribution and tracers of the dark matter distribution on large spatial scales.[22] This kind of detection has been recently achieved by using Planck data and appropriate tracers; see Ref. 31, where it is claimed that some detected cross-correlations are compatible with the ΛCDM predictions; although other models may also be admissible. Previous detections are also listed in Ref. 31.

Since the LISW effects are distinct in the ΛCDM model of GR and in AR-VTG with $D = 4 \times 10^8$, with small relative differences (reaching values close to 6%), as it has been mentioned at the beginning of this section, the cross correlations predicted in the contexts of both models should be also different although comparable and; then, the question is: Could we select one of these models by comparing the cross-correlations predicted in them with those observed? Could we do that with high statistical significance? In Sec. 3.1. we have outlined what could be a continuity way for this research, in such a case, we should use more complex models and estimators. A deep study on this line is out of the scope of this paper, but could lead to the selection of one of the AR-VTG models in future.

Acknowledgments

This work has been supported by the Spanish Ministry of *Economía y Competitividad*, MINECO-FEDER project FIS2015-64552-P and CONSOLIDER-INGENIO project CSD2010-00064. Calculations were carried out at the Centre de Càlcul de la Universitat de València. Unfortunately Professor Diego Sáez passed away during the writing of this paper. On behalf of myself and my colleague Diego (R.I.P.), I want to thank Pier-Stefano Corasaniti which has generously provide the CROSS-CMBFAST original code.

References

1. Planck Collab. (P. A. R. Ade *et al.*), *Astron. Astrophys.* **594** (2016) A14.
2. C. M. Will, *Theory and Experiment in Gravitational Physics* (Cambridge University Press, Cambridge, 1993).
3. C. M. Will, *Living Rev. Rel.*. **9** (2006) 3.
4. R. Dale, J. A. Morales and D. Sáez, arXiv:0906.2085 [astro-ph].
5. R. Dale and D. Sáez, *Phys. Rev. D* **85** (2012) 124047.
6. R. Dale and D. Sáez, *Phys. Rev. D* **89** (2014) 044035.
7. R. Dale and D. Sáez, *J. Cosmol. Astropart. Phys.* **01** (2017) 004.
8. R. Dale, M. J. Fullana and D. Sáez, *Astrophys. Space Sci.* **357** (2015) 116.
9. L. Heisenberg, *J. Cosmol. Astropart. Phys.* **05** (2014) 015.

10. J. M. Bardeen, *Phys. Rev. D* **22** (1980) 1882.
11. W. Hu and M. White, *Phys. Rev. D* **56** (1997) 596.
12. C. P. Ma and E. Bertschinger, *Astrophys. J.* **455** (1995) 7.
13. M. J. Fullana *et al.*, *Mon. Not. R. Astron. Soc.* **464** (2017) 3784.
14. W. Hu and N. Sugiyama, *Phys. Rev. D* **50** (1994) 627.
15. M. Zaldarriaga and D. D. Harari, *Phys. Rev. D* **52** (1995) 3276.
16. A. Lewis, A. Challinor and A. Lasenby, *Astrophys. J.* **538** (2000) 473.
17. C. M. Will and K. Nordtvedt Jr., *Astrophys. J.* **177** (1972) 757.
18. R. W. Hellings and K. Nordtvedt Jr., *Phys. Rev. D* **7** (1973) 3593.
19. J. B. Jimnez and A. L. Maroto, *J. Cosmol. Astropart. Phys.* **03** (2009) 016.
20. A. Lewis and S. Bridle, *Phys. Rev. D* **66** (2002) 103511.
21. Planck Collab. (P. A. R. Ade *et al.*), *Astron. Astrophys.* **594** (2016) A13.
22. R. G. Critteden and N. Turok, *Phys. Rev. Lett.* **76** (1996) 575.
23. R. Scranton *et al.*, arXiv:astro-ph/0307335.
24. P. Corasaniti, T. Giannantonio and A. Melchiorri, *Phys. Rev. D* **71** (2005) 123521.
25. F. Schiavon *et al.*, *Mon. Not. R. Astron. Soc.* **427** (2012) 3044.
26. J. Lesgourgues, W. Valkenburg and E. Gaztañaga, *Phys. Rev. D* **77** (2008) 063505.
27. G. Olivares, F. Atrio-Barandela and D. Pavón, *Phys. Rev. D* **77** (2008) 103520.
28. A. Lue, R. Scoccimarro and G. D. Starkman, *Phys. Rev. D* **69** (2004) 044005.
29. Y. S. Song, I. Sawicki and W. Hu, *Phys. Rev. D* **75** (2007) 064003.
30. U. Seljak and M. Zaldarriaga, *Astrophys. J.* **469** (1996) 437.
31. Planck Collab. (P. A. R. Ade *et al.*), *Astron. Astrophys.* **571** (2014) A19.